Exact Principal Mode Field for a Lossy Coaxial Line

William C. Daywitt

Abstract—**Exact field equations for a lossy coaxial transmission line with an infinite outer conductor are presented. The corresponding determinantal equation is solved to obtain an exact propagation constant from which errors in the usual microwave approximation and an alternative full frequency range approximation are calculated. The calculations show that the microwave approximation, although containing a large relative error at the lower frequencies, is still useful in practical applications.**

Keywords—**coaxial transmission line; Maxwell's equations; principal mode; propagation constant; telegrapher equation.**

I. Introduction

An exact field solution to Maxwell's equations for a coaxial transmission line has been in existence since at least 1941 [1], but has gone unrecognized or at least unexploited since that time. This is probably because in 1941 the means of calculation available today were nonexistent so the exact solution was inadvertently buried in the need to approximate. In any case, this solution has been recently developed and is presented in this paper.

As six-port and automatic network analyzers have become more accurate and sensitive and are being utilized at lower and lower frequencies, increasing emphasis is placed upon accuracy of the transmission line standards used to characterize or calibrate these systems. In particular, accurate calculation of the line's propagation constant acquires added importance. The approximation used at present [1], [2] to calculate this constant, however, needs to be reexamined below the microwave frequency region for which it was derived since its accuracy could only be estimated in the past from Russell's equations [3], which themselves are approximate. The work described here was pursued in part to correct this situation and represents the first real check on the microwave approximation; it also suggests an alternative approximation to the propagation constant that is more accurate and that is applicable over the full frequency range of the line.

Russell's 1909 paper [3], which was used [2] to estimate the accuracy of the microwave approximation to the propagation constant and the distributed line parameters, is interesting in its own right. It discusses early theoretical developments concerning the transmission of high-frequency currents down "concentric mains" (involving the efforts of Maxwell, Heaviside, and Lord Rayleigh) and contributes significantly to that development in addition to deriving approximations to Kelvin's "ber," "bei," "ker," and "kei" functions that are standard today. The approximations in Russell's solution appear in his equations (59)–(61), where Faraday's, Ohm's, and an integral form of Ampere's law (not the exact version containing the displacement current) are used in addition to the approximation that the axial electric field is constant across the conductors.

The establishment of impedance standards for integrated circuit applications in stripline and microstrip transmission lines is considerably more difficult than similar endeavors for coaxial lines such as the one described here. Indeed, even an accurate description of the wave propagation on these miniature lines is complex, and it is useful to have at least one exact transmission line solution against which to compare results. The fields and results to be described below constitute one of these exact solutions.

The exact coaxial line solution is presented in the next section, preceding which is a short review of the pertinent theory that is included to collect the equations in one place and because of the importance of air line standards to precision network analyzer calibrations. A slight change has been made in the derivation to avoid divergences present in the usual treatment [1] as the frequency or the conductor resistivity approaches zero.

Boundary conditions requiring continuity of the fields tangential to the conducting surfaces are applied in Section III to derive the determinantal equation, and a simple iteration scheme to quickly find the root (which is used to calculate the propagation constant) is presented.

Approximations are developed in Section IV, where an expression for the root of the determinantal equation is presented that is more accurate and applies over a wider frequency range than the microwave version [1], [2] presently in use. Full range, first-order fields are also presented in that section.

A number of results are discussed in Section V, including field graphs within and without the conductors; a comparison of the conductor skin depths with the planar approximation; graphs showing the accuracy of the approximations, in particular the accuracy of the propaga-

Manuscript received January 15, 1991; revised April 9, 1991.

The author is with the National Institute of Standards and Technology, 325 Broadway, Boulder, CO 80303.

IEEE Log Number 9101008.

U.S. Government work not protected by U.S. copyright

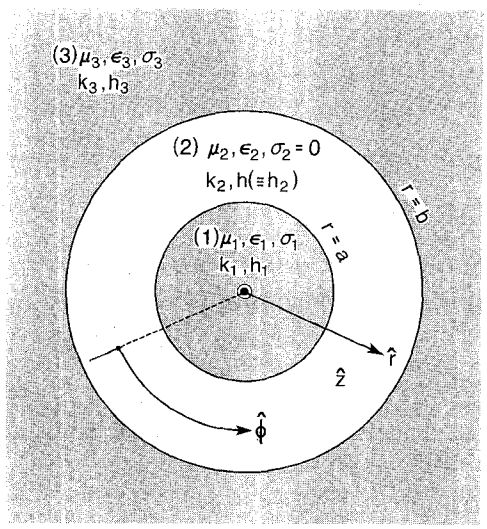

Fig. 1. Cross-sectional view of a coaxial transmission line with an infinite outer conductor.

tion constant calculations; a comparison of the inner and outer conductor currents; and, finally, graphs of the wave impedance and phase velocity versus frequency. Conclusions drawn from the results are presented in Section VI.

II. Exact Fields

A derivation of the exact electric and magnetic fields propagating along the axis of a coaxial line is briefly reviewed in this section. The line (Fig. 1) is assumed to be homogeneous and isotropic with a uniform cross section consisting of a center conductor (region 1), a dielectric region between the conductors (region 2), and an outer conductor (region 3). The magnetic permeabilities, electric permittivities, and conductivities are denoted by μ_i, ϵ_i, and σ_i in the various regions ($i = 1,2,3$) and $\sigma_2 = 0$ in the dielectric region 2. The wavenumbers are denoted by k_i, and the h_i are parameters to be described later. The coordinate system is right-handed with the directions $(\hat{r}, \hat{\phi}, \hat{z})$ shown in the figure, the z direction coming out of the paper toward the reader. The conductor resistivities are denoted by ρ_i ($\equiv 1/\sigma_i$) and will be used instead of the conductivities when convenient.

The three regions are assumed to be source free so that Maxwell's equations in SI units take the form

$$\nabla \times \boldsymbol{E} = -j\omega\mu_i \boldsymbol{H} \qquad \nabla \cdot \boldsymbol{B} = 0 \tag{1}$$

$$\nabla \times \boldsymbol{H} = (\sigma_i + j\omega\epsilon_i)\boldsymbol{E} \qquad \nabla \cdot \boldsymbol{E} = 0 \tag{2}$$

where the harmonic variation $e^{j\omega t}$ is assumed. Performing the standard vector operations [1] on (1) and (2) leads to the Helmholtz equation

$$\left[\nabla^2 + \left(\omega^2\mu_i\epsilon_i - j\omega\mu_i\sigma_i\right)\right]\begin{Bmatrix} \boldsymbol{E} \\ \boldsymbol{H} \end{Bmatrix} = 0 \tag{3}$$

that must be satisfied by the $\boldsymbol{E}$ and $\boldsymbol{H}$ fields.

The Laplacian in (3) is separable into transverse and longitudinal components, corresponding respectively to the $\hat{r}$ and $\hat{\phi}$ and to the $\hat{z}$ directions in cylindrical coordinates. Furthermore, (3) implies that each cylindrical component of both $\boldsymbol{E}$ and $\boldsymbol{H}$ must satisfy this Helmholtz equation and have the form [4]

$$\Psi(r,\phi,z) = R(r)\Phi(\phi)e^{-\gamma z} \tag{4}$$

where γ is a separation constant. Inserting (4) into (3) after expressing the Laplacian in cylindrical coordinates produces an equation that is separable into the two equations

$$r^2R''(r) + rR'(r) + \left(h_i^2 r^2 - n^2\right)R(r) = 0 \tag{5}$$

and

$$\Phi''(\phi) = -n^2\Phi(\phi). \tag{6}$$

The separation constant n is chosen to be 0 since the principal mode magnet field does not vary in the $\hat{\phi}$ direction. The h_i in (5) is another separation constant, given by

$$h_i^2 \equiv k_i^2 + \gamma^2 \tag{7}$$

where the complex wavenumber, k_i, is

$$k_i^2 \equiv \omega^2\mu_i\epsilon_i - j\omega\mu_i\sigma_i. \tag{8}$$

Solutions to (5) that are of interest are the Bessel functions of the first, second, and third kinds; $J_n(hr)$, $N_n(hr)$, and $H_n^{(2)}(hr)$ (Hankel function). The index n will take on the values 0 and 1, the 1 appearing because of the derivatives in (5) even though only $n = 0$ is needed in (6) to satisfy the symmetry requirement of the magnetic field in the $\hat{\phi}$ direction.

The preceding equations are applied to each of the three coaxial regions using a different h_i (h_1, h_2, or h_3) and k_i (k_1, k_2, or k_3) for each region. Various combinations of the Bessel functions are used to satisfy boundary conditions and generate finite fields at $r = 0$ and $r = \infty$, leading to the following three sets of fields (the common factor $\exp(j\omega t - \gamma z)$ has been suppressed from the equations):

Region 1 ($r \leqslant a$)

$$\begin{Bmatrix} E_r \\ E_z \\ H_\phi \end{Bmatrix} = C_1 \begin{cases} J_1(h_1 r), & r < a \\ h_1\gamma^{-1}J_0(h_1 r), & r \leqslant a \\ Y_1 J_1(h_1 r), & r \leqslant a. \end{cases} \tag{9}$$

Region 2 ($a \leqslant r \leqslant b$, $h \equiv h_2$)

$$\begin{Bmatrix} E_r \\ E_z \\ H_\phi \end{Bmatrix} = C_2 \begin{cases} Z_1(hr), & a < r < b \\ h\gamma^{-1}Z_0(hr), & a \leqslant r \leqslant b \\ Y_2 Z_1(hr), & a \leqslant r \leqslant b. \end{cases} \tag{10}$$

Region 3 ($b \leqslant r$)

$$\begin{Bmatrix} E_r \\ E_z \\ H_\phi \end{Bmatrix} = C_3 \begin{cases} H_1^{(2)}(h_3 r), & b < r \\ h_3\gamma^{-1}H_0^{(2)}(h_3 r), & b \leqslant r \\ Y_3 H_1^{(2)}(h_3 r), & b \leqslant r. \end{cases} \tag{11}$$

The constants C_1, C_2, and C_3 have the units of volts per meter but are for the present arbitrary. The constants h_1

and h_3 are calculated from

$$h_i = \left(k_i^2 + \gamma^2\right)^{1/2} \tag{12}$$

where k_1, k_2 (with $\sigma_2 = 0$), and k_3 are given by

$$k_i \equiv \left(\omega^2 \mu_i \epsilon_i - j\omega\mu_i\sigma_i\right)^{1/2} \tag{13}$$

with $i = 1,2,3$. The wave admittances are

$$Y_i = \frac{jk_i^2}{\omega\mu_i\gamma} \tag{14}$$

and the propagation constant is calculated from

$$\gamma = \left(h^2 - k_2^2\right)^{1/2} = jk_2\left(1 - h^2/k_2^2\right)^{1/2}. \tag{15}$$

The quantity h is obtained from the determinantal equation (28) discussed in the next section.

The Z_n $(n = 0,1)$ functions in (10) are defined by the equation

$$Z_n(hr) \equiv GJ_n(hr) + hbN_n(hr) \tag{16}$$

where G is a constant determined by the boundary conditions. This last definition was chosen in place of the usual definition, $Z_n = J_n + GN_n$ [1], to avoid divergences in both G and N_n as h approaches 0 owing to the frequency or the conductor losses (resistivities) approaching 0. Both terms in (16) are well behaved in these limits, the first term approaching 0 and the second term approaching 0 or $-2b/\pi r$ depending on whether $n = 0$ or $n = 1$.

Each set of fields given by (9), (10), and (11) satisfies Maxwell's equations identically, as can be seen by substitution into (1) and (2), using the Bessel function recursion relations to reduce the resulting terms containing $n = 2$ to combinations of terms containing only $n = 0$ or $n = 1$.

The boundary conditions require the continuity of E_z and H_ϕ at $r = a, b$, and yield the following field expressions which are obtained from the fields in (9)–(11) by solving the boundary conditions for C_1 and C_3 in terms of C_2 and using (14) for the wave admittances:

Region 1:

$$E_r = C_2 \frac{\mu_1 k_2^2}{\mu_2 k_1^2} Z_1(ha) \frac{J_1(h_1 r)}{J_1(h_1 a)} e^{-\gamma z} \tag{17}$$

$$E_z = C_2 \frac{h}{\gamma} Z_0(ha) \frac{J_0(h_1 r)}{J_0(h_1 a)} e^{-\gamma z} \tag{18}$$

$$H_\phi = Y_1 E_r. \tag{19}$$

Region 2:

$$E_r = C_2 Z_1(hr) e^{-\gamma z} \tag{20}$$

$$E_z = C_2 \frac{h}{\gamma} Z_0(hr) e^{-\gamma z} \tag{21}$$

$$H_\phi = Y_2 E_r. \tag{22}$$

Region 3:

$$E_r = C_2 \frac{\mu_3 k_2^2}{\mu_2 k_3^2} Z_1(hb) \frac{H_1^{(2)}(h_3 r)}{H_1^{(2)}(h_3 b)} e^{-\gamma z} \tag{23}$$

$$E_z = C_2 \frac{h}{\gamma} Z_0(hb) \frac{H_0^{(2)}(h_3 r)}{H_0^{(2)}(h_3 b)} e^{-\gamma z} \tag{24}$$

$$H_\phi = Y_3 E_r. \tag{25}$$

Magnetic losses within the conductors and dielectric losses between the conductors can be included by using a complex μ_1, μ_3, and k_2.

The field expressions (17)–(25) formally satisfy both Maxwell's equations and the boundary conditions exactly, but the value of h must still be determined in order to calculate the propagation constant γ and complex fields. This is accomplished in the next section.

III. Determinantal Equation

Calculation of the constant h is necessary to utilize the field equations of the last section. It is obtained, like the C_i constants, by applying boundary conditions at $r = a$ and $r = b$. The resulting equation from which h is determined and a simple means of solving that equation are described in this section.

Two expressions containing the constants C_1 and C_2 are obtained by requiring continuity in E_z and H_ϕ at the boundary $r = a$ (see (9)–(11)). Eliminating these constants between the two expressions yields

$$\frac{Z_0(ha)}{Z_1(ha)} = \frac{\mu_1 k_2^2 h_1 J_0(h_1 a)}{\mu_2 k_1^2 h J_1(h_1 a)}. \tag{26}$$

A similar equation is obtained by requiring continuity at $r = b$:

$$\frac{Z_0(hb)}{Z_1(hb)} = \frac{\mu_3 k_2^2 h_3 H_0^{(2)}(h_3 b)}{\mu_2 k_3^2 h H_1^{(2)}(h_3 b)}. \tag{27}$$

Both (26) and (27) contain the constant G implicitly in their respective Z_n's, each yielding an equation for G when the Z_n's are replaced by their equivalents in (16):

$$G = \frac{\mu_2^{-1} k_2^2 hbN_1(ha) - \left(\mu_1^{-1} k_1^2 / h_1\right) h^2 b R_1(h_1 a) N_0(ha)}{\left(\mu_1^{-1} k_1^2 / h_1\right) h R_1(h_1 a) J_0(ha) - \mu_2^{-1} k_2^2 J_1(ha)}$$
$$= \frac{\mu_2^{-1} k_2^2 hbN_1(hb) - \left(\mu_3^{-1} k_3^2 / h_3\right) h^2 b R_3(h_3 b) N_0(hb)}{\left(\mu_3^{-1} k_3^2 / h_3\right) h R_3(h_3 b) J_0(hb) - \mu_2^{-1} k_2^2 J_1(hb)} \tag{28}$$

where

$$R_1(h_1 a) \equiv \frac{J_1(h_1 a)}{J_0(h_1 a)} \qquad R_3(h_3 b) \equiv \frac{H_1^{(2)}(h_3 b)}{H_0^{(2)}(h_3 b)}. \tag{29}$$

The last equality in (28) is the *determinantal equation* from which the root h is extracted. There are actually an infinity of roots: the root with magnitude close to 0 which is the desired h of the principal mode; and an infinite number of other roots with nonzero magnitudes that

belong to the symmetric TM waveguide modes [1], [5], which are of no interest in the present work.

A simple and rapidly convergent iteration scheme for finding the root h of (28) can be obtained with the following seven steps:

1) make an initial estimate for h using (32) in (35);
2) calculate h_1 and h_3 from the results of step 1 and (12);
3) calculate $R_1(h_1a)$ and $R_3(h_3b)$ from the results of step 2 and (29);
4) calculate the right and left sides of the second equality in (28) from the results in steps 1, 2, and 3;
5) calculate the difference δG between the calculations in step 4 and the correction to h using

$$\delta h = \frac{\pi \delta G}{2b}\left[\ln\frac{b}{a} + \frac{k_2^2}{h^2}\left(\frac{1}{k_1 a R_1} - \frac{1}{k_3 b R_3}\right)\right]^{-1}; \quad (30)$$

6) add the correction δh to the h estimated in step 1;
7) finally, iterate steps 2 through 6 until the desired accuracy in h is achieved.

Three iterations are sufficient to produce an h accurate to approximately 14 significant figures for the numerical example in Section V. The formula in (30) was obtained by differentiating the difference between the two sides of the last equation in (31) with respect to h (note that the logarithm of h cancels when taking the difference).

Once h is found, h_1 and h_3 can be calculated from (12) after the propagation constant γ is calculated from (15).

IV. Approximations

The exact expressions found in the previous two sections are inconvenient to use in many practical applications because of the effort and time required for their calculation, so accurate approximations are often necessary. Some of the more important approximations are presented in this section.

The following two approximations ($\hat{G}$) for G can be obtained by dropping the k_2^2 terms in the denominators of (28):

$$\hat{G} = \frac{2hb}{\pi}\left(\ln\frac{2}{cha} - \frac{\mu_1 k_2^2}{\mu_2 k_1 h^2 a R_1}\right)$$

$$= \frac{2hb}{\pi}\left(\ln\frac{2}{chb} - \frac{\mu_3 k_2^2}{\mu_2 k_3 h^2 b R_3}\right) \quad (31)$$

where $c \equiv \exp(0.5772156649\cdots)$ and $0.5772156649\cdots$ is Euler's constant; where

$$R_1 \equiv R_1(k_1 a) \qquad R_3 \equiv R_3(k_3 b) \quad (32)$$

and where the following approximations have been made for small $z(\equiv hr)$:

$$J_0(z) \doteq 1 - z^2/4$$
$$J_1(z) \doteq z/2 \quad (33)$$

$$N_0(z) \doteq -\frac{2}{\pi}\left(\ln\frac{2}{cz}J_0(z) - \frac{z^2}{4}\right)$$

$$N_1(z) \doteq -\frac{2}{\pi}\left(\frac{1}{z} + \frac{z}{2}\ln\frac{2}{cz} + \frac{z}{4}\right). \quad (34)$$

After making the substitutions (32)–(34) it is necessary to examine the magnitude of each of the resulting terms, discarding those which are insignificant compared with the rest, to arrive at (31). Equation (31) corresponds to Stratton's equation (39) on page 551 of [1].

Solving (31) for h yields the following approximation $\hat{h}$:

$$\frac{\hat{h}^2}{k_2^2} = \frac{\mu_1/k_1 a R_1 - \mu_3/k_3 b R_3}{\mu_2 \ln(b/a)} \quad (35)$$

which can be substituted back into (31) for h to obtain $\hat{G}$. This approximation will apply over the full frequency range of the transmission line and is Stratton's equation (40) on page 552 of [1] (Stratton's λ corresponds to the h used in the present paper). It is seen to contain k_1 and k_3 explicitly and implicitly via the functions R_1 and R_3, the latter preventing (35) from being a simple proportion in $1/k_1$ and $1/k_3$. In contrast to (35), substituting

$$R_1 \doteq -j \qquad R_3 \doteq j \quad (36)$$

leads to the usual, microwave approximation h_0:

$$\frac{h_0^2}{k_2^2} = \frac{j(\mu_1/k_1 a + \mu_3/k_3 b)}{\mu_2 \ln(b/a)} \quad (37)$$

where if $k_1 = k_3$, then h_0 is proportional to the reciprocal of k_i or the normalized surface impedance of the conductors (see (A5)). This approximation gives good accuracy only at the upper, microwave end of the line's frequency range. This is the solution that has survived since 1941 and that is in common usage today [1]. The positive square roots in (35) and (37) are taken when $\hat{h}$ and h_0 are required.

Equation (31) is a "small h" approximation to G whereas the corresponding microwave expression is a first-order approximation in the metallic surface impedance of the conductors, approximating R_1 and R_3 (36) in addition to the approximations (33) and (34). This distinction is what makes the newer approximations full frequency range approximations, i.e., usable and accurate from 0 Hz to the upper usable frequency of the transmission line (e.g. 18 GHz for the 7 mm, 50 Ω line).

The approximate full range propagation constant $\hat{\gamma}$ is obtained by using (35) in the second expression of (15):

$$\hat{\gamma} = jk_2\left(1 - \hat{h}^2/2k_2^2\right). \quad (38)$$

This result permits the line loss and phase shift to be accurately calculated over the full frequency range of the line once R_1 and R_3 are determined (see the Appendix).

Region 2 Fields

With $C_2 \equiv -\pi/2$, the following approximations to (20)–(22) can be derived:

$$E_r = \frac{b(1+re_r)}{r} e^{-\hat{\gamma}z} \tag{39}$$

$$E_z = \frac{2b}{\gamma_{00} r^2}\left(re_r - \frac{\hat{h}^2 r^2}{4}\right) e^{-\hat{\gamma}z} \tag{40}$$

and

$$H_\phi = Y_{20}\frac{b}{r}\left(1 + \frac{\delta Y_2}{Y_{20}} + re_r\right) e^{-\hat{\gamma}z} \tag{41}$$

where

$$re_r \equiv \frac{\hat{h}^2 r^2}{2}\left(\ln\frac{b}{r} + \frac{1}{2} - \frac{\ln(b/a)}{1 - \mu_1 k_3 b R_3/\mu_3 k_1 a R_1}\right) \tag{42}$$

$$\hat{\gamma} = \gamma_{00} + \delta\gamma \tag{43}$$

$$\gamma_{00} \equiv jk_2 \qquad Y_{20} = \frac{k_2}{\omega\mu_2} \tag{44}$$

and

$$\frac{\delta\gamma}{\gamma_{00}} = -\frac{\delta Y_2}{Y_{20}} = -\frac{\hat{h}^2}{2k_2^2}. \tag{45}$$

The fields given by (39)–(41) are complete solutions to first order in the squared quantity h^2 in the sense that, if substituted into Maxwell's equations (1) and (2) with the results reduced to first order, they satisfy those equations identically. They are related to the corresponding equations in [5], which are complete microwave solutions to first order in the surface impedance. The significant difference is the appearance of R_1 and R_3 in place of $-j$ and j in the earlier definition of re_r in [5].

V. Numerical Results

The theoretical results of the previous three sections are illustrated in this section by numerical examples calculated for a 7 mm, 50 Ω line. The line is assumed to have a resistivity of 2 $\mu\Omega\cdot$cm, corresponding to equal inner and outer conductor conductivities (σ_1, σ_3) of 5×10^7 S/m, a value that is roughly representative of copper, silver, and gold. The other constitutive parameters that were used for the calculations are $\sigma_2 = 0$, $\mu_1 = \mu_2 = \mu_3 = \mu_0$, and $\epsilon_1 = \epsilon_2 = \epsilon_3 = \epsilon_0$. Results for other line sizes are similar to the ones shown below.

A. Fields, h, Skin Depths

The magnetic field described by (19), (22), and (25) is plotted in Fig. 2 for various frequencies as a function of the radius r. The magnitude is normalized by its maximum value at $r = a$ and the radius by the inner conductor radius a. The fields between $r = a$ and $r = b$ at the various frequencies differ a small amount because of conductor loss, but the vertical scale of the graph is too coarse to show this effect. The 1 Hz line is close to the direct current case, exhibiting a linear falloff in the center conductor and a $1/r$ falloff in the outer conductor. The dashed levels at $1/e$ and $0.434/e$ will be used later in discussing the skin depth.

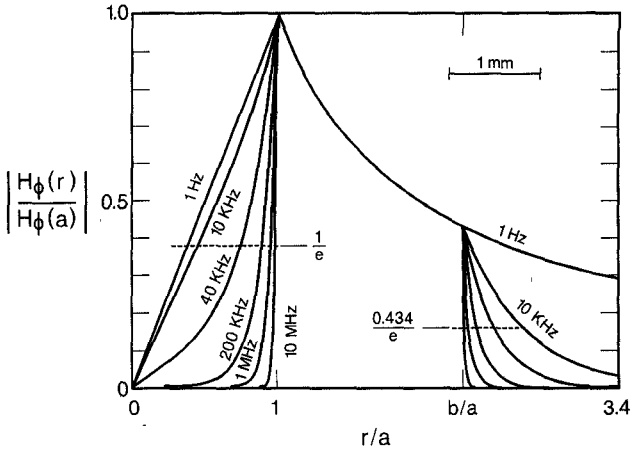

Fig. 2. Graph of the normalized magnetic field as a function of the normalized radius for various frequencies.

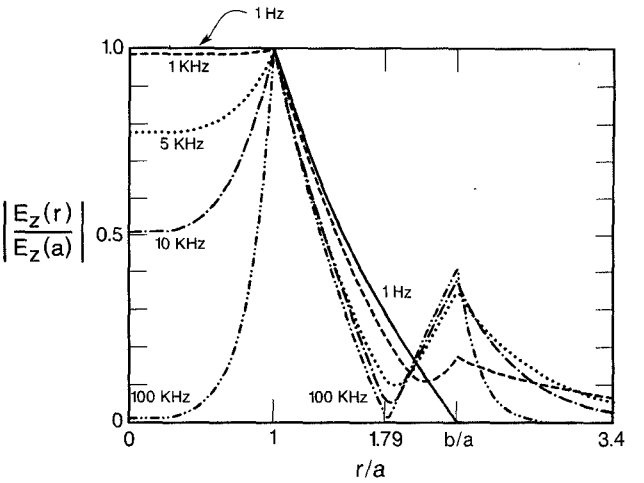

Fig. 3. Graph of the normalized longitudinal electric field as a function of the normalized radius for various frequencies.

Fig. 3 is a graph of the longitudinal electric field (E_z) magnitude as a function of r for various frequencies. It is interesting to note that the magnitude does not vanish between the conductors, a feature that is evident in the approximate equation (40) also. The local minima, however, are seen to approach 0 at $r \doteq 1.79$ (a value easily derived from (40)) as the frequency is increased.

Fig. 4 is a graph of the phase angle of E_z between the conductors. The phase remains relatively constant with frequency until a transition region around 1.79 is reached, at which point it abruptly changes by approximately 180°. This phase reversal is sufficient to ensure that there is a positive average Poynting flux into the conductors at both $r = a$ and $r = b$, accounting for the inner and outer conductor losses.

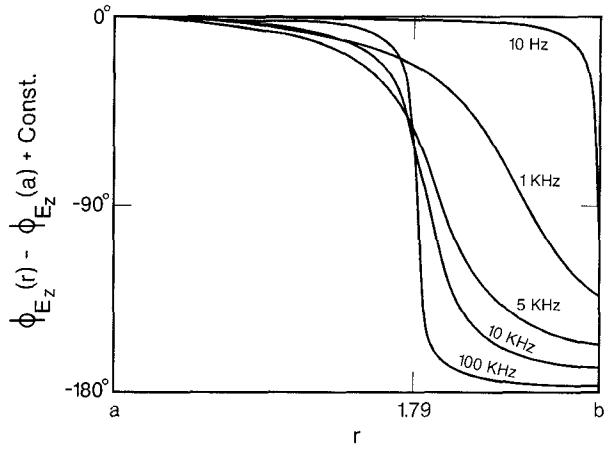

Fig. 4. Graph of the phase of the normalized longitudinal electric field as a function of the normalized radius for various frequencies.

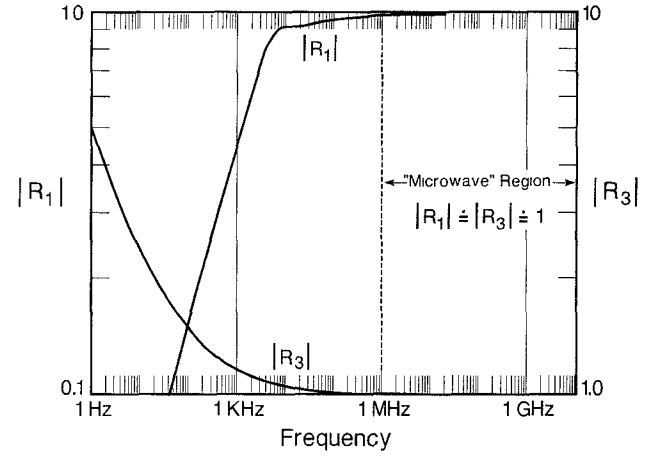

Fig. 6. Graph of the magnitude of R_1 and R_3 as a function of frequency.

TABLE I
CONVERGENCE OF THE PARAMETER h AT 18 GHz

Re(h)	Im(h)
0.0297441614416505	0.0718037438397921
0.0297448538545143	0.0718040306557353
0.0297448539891355	0.0718040305999745
0.0297448539891461	0.0718040305999490
0.0297448539891461	0.0718040305999490

Calculated using $h_1 = k_1$ and $h_3 = k_3$.

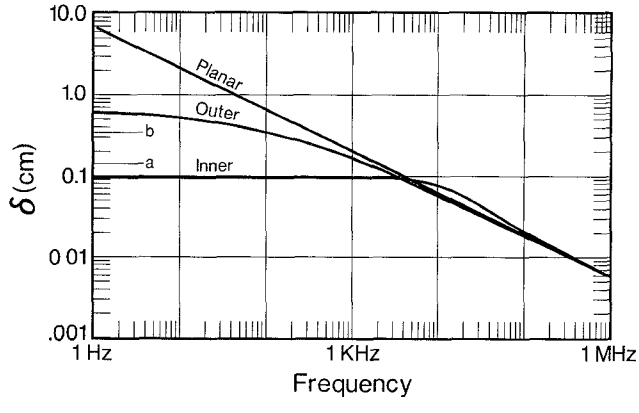

Fig. 5. Graph of the skin depths as a function of frequency.

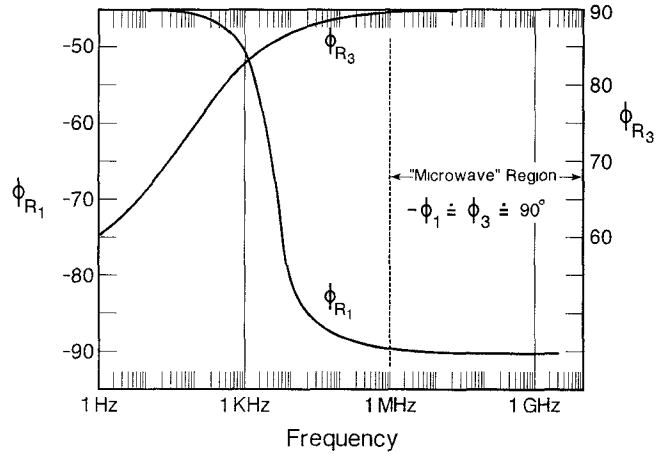

Fig. 7. Graph of the phase of R_1 and R_3 as a function of frequency.

Table I illustrates the rapidity with which the iteration scheme for finding the root h of the determinantal equation discussed in Section III converges. The real and imaginary parts of h shown in the first row are the equation (35) estimates. The convergence is seen to be 15 significant figures in three iterations.

The skin depth is defined as that distance *into* the conductors at which the magnitudes of H_ϕ or E_r fall to $1/e$ (see the dashed levels in Fig. 2) of their respective values at the surface of the conductors. It is generally different for the two conductors, but this difference is not significant in the microwave frequency region of the line. Fig. 5 shows the skin depth as a function of frequency and includes the usual microwave or planar approximation [6] in addition to the inner and outer conductor skin depths.

The outer conductor skin depth is generally less than the planar approximation because the fields are spreading out as r increases so it requires a shorter distance for the $1/e$ falloff to occur. An opposite effect holds for the inner conductor until a crossover at approximately 7 kHz. The crossover and the fact that both inner and outer conductor skin depths become constant as the frequency decreases can be seen by examining Fig. 2, an exercise left to the reader.

B. Approximations

The microwave and full range approximations differ by the $R_1 \doteq -j$ and $R_3 = j$ approximations used in deriving the former. Figs. 6 and 7 are graphs of the magnitudes and angles of R_1 and R_3 as a function of frequency. They show that the magnitudes begin to diverge from their microwave approximations at about 1 MHz and the angles begin to diverge somewhere between 1 and 10 MHz. Thus, for a 7 mm line the microwave approximations start to fail as the frequency drops below about 1 MHz. Using this 1 MHz cutoff point for the argument of (A6) leads to

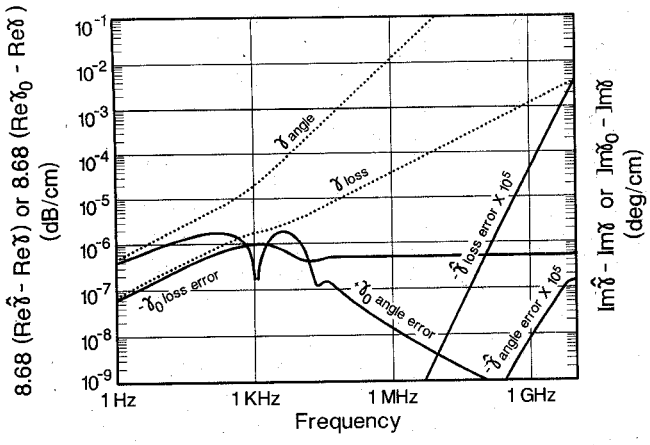

Fig. 8. Graph of γ and the errors in $\hat{\gamma}$ and γ_0 as a function of frequency.

the rule-of-thumb relation $f=(0.15/a)^2$ (a in cm and f in MHz) as the point where failure begins for any line of inner conductor radius a. For example, a 3.5 mm line starts at 4 MHz.

Fig. 8 shows the errors using the microwave (γ_0) and full range ($\hat{\gamma}$) approximations to the line loss per unit length and the phase angle per unit length as a function of frequency. The line loss errors, 8.68 ($\mathrm{Re}\,\gamma_0-\mathrm{Re}\,\gamma$) and 8.68 ($\mathrm{Re}\,\hat{\gamma}-\mathrm{Re}\,\gamma$), are in units of dB/cm; and the angle errors, $\mathrm{Im}\,\gamma_0-\mathrm{Im}\,\gamma$ and $\mathrm{Im}\,\hat{\gamma}-\mathrm{Im}\,\gamma$, are in units of degrees/cm. The errors in the full range approximations are multiplied by a factor of 10^5 to bring them up onto the scale of the graph. The absolute loss and angle calculated from the exact γ are also shown for comparison. The sharp dip in the γ_0 curve is due to a change of sign in that error. The errors at 18 GHz are 6.2×10^{-7} dB/cm and 8.2×10^{-11} deg/cm for γ_0 and 1.3×10^{-7} dB/cm and 3.8×10^{-12} deg/cm for $\hat{\gamma}$. It is clear from the graph that the full range errors sharply decrease as the frequency decreases, while the microwave errors become increasingly significant.

The dotted γ curves in Fig. 8 also show how the real and imaginary parts of the propagation constant vary in the limits of high and low frequencies. The curves are linear in these limits, indicating a power law dependence with frequency for both real and imaginary components. In the high-frequency limit the phase angle varies linearly with frequency while the loss component varies as the square root of the frequency. In the low-frequency limit both components vary as the square root of the frequency. These results can be compared with [7, fig. 5.19] and explain how both α and β approach zero in that figure.

The error in the full range approximations of the fields in region 2 is greatest at the highest usable line frequency. Table II shows a comparison between the exact and approximate field values for a radius of $1.5a$ and a frequency of 18 GHz. (The magnitudes have arbitrary units and the phases are in units of degrees, while the magnitude error is a relative error and the phase error has the units of degrees.) The errors decrease rapidly as the frequency decreases.

C. Conductor Currents

It proves interesting to calculate the total conductor currents since we are now in possession of the exact fields. The first equation in (2) takes the form

$$\boldsymbol{J}=\nabla\times\boldsymbol{H}-j\omega\epsilon\boldsymbol{E} \tag{46}$$

when $\sigma\boldsymbol{E}$ is replaced by the current density within the conductors. Using (46) and the Bessel function recursion relations, it is straightforward to show that the currents in the center and outer conductors are

$$I_1=\int_0^{2\pi}\int_0^a \boldsymbol{J}\cdot d\boldsymbol{S}$$
$$=2\pi aH_\phi(a)-2\pi j\omega\epsilon_1\frac{ha}{\gamma h_1}Z_0(ha)R_1(h_1a) \tag{47}$$

and

$$I_3=\int_0^{2\pi}\int_b^\infty \boldsymbol{J}\cdot d\boldsymbol{S}$$
$$=-2\pi bH_\phi(b)+2\pi j\omega\epsilon_3\frac{hb}{\gamma h_3}Z_0(hb)R_3(h_3b) \tag{48}$$

respectively. Simpler expressions for the currents can be obtained by performing the integrations again with $\boldsymbol{J}=\sigma\boldsymbol{E}$ in place of (46), leading to

$$I_1=\frac{2\pi a\sigma_1E_z(a)R_1(h_1a)}{h_1} \tag{49}$$

and

$$I_3=-\frac{2\pi b\sigma_3E_z(b)R_3(h_3b)}{h_3} \tag{50}$$

which can be used to simplify the second terms of (47) and (48). Inserting (49) into (47) for R_1/h_1 and (50) into (48) for R_3/h_3 gives

$$I_1=\frac{2\pi aH_\phi(a)}{1+j\omega\epsilon_1/\sigma_1}\qquad I_3=-\frac{2\pi bH_\phi(b)}{1+j\omega\epsilon_3/\sigma_3} \tag{51}$$

and

$$\frac{I_3}{I_1}=-\frac{bH_\phi(b)}{aH_\phi(a)}\left(\frac{1+j\omega\epsilon_1/\sigma_1}{1+j\omega\epsilon_3/\sigma_3}\right). \tag{52}$$

Equation (52) becomes

$$\frac{I_3}{I_1}=-\frac{bH_\phi(b)}{aH_\phi(a)} \tag{53}$$

for similar inner and outer conductors where $\epsilon_1=\epsilon_3$ and $\sigma_1=\sigma_3$.

The effect of the displacement current (the denominators in (51)) on the total conductor current is to slightly decrease the magnitude of their magnetically ($\boldsymbol{H}$ field) induced components (the numerators of (51)) and to retard their phases. The ratio in (52) shows that the

TABLE II
ACCURACY OF THE FIRST ORDER FULL RANGE FIELDS AT $r/a = 1.5$ FOR 18 GHz

	Magnitude	Phase	Magnitude Error	Phase Error
Exact E_r	9.77194E-1	−179.996		
Approx E_r	9.77194E-1	−179.996	1.3E-12	3.7E-7
Exact E_z	6.28027E-5	−134.998		
Approx E_z	6.28063E-5	−135.001	5.8E-5	−3.4E-3
Exact H_ϕ	2.59349E-3	−179.987		
Approx H_ϕ	2.59439E-3	−179.987	9.8E-12	5.3E-6

Calculated using $h_1 = k_1$ and $h_3 = k_3$.

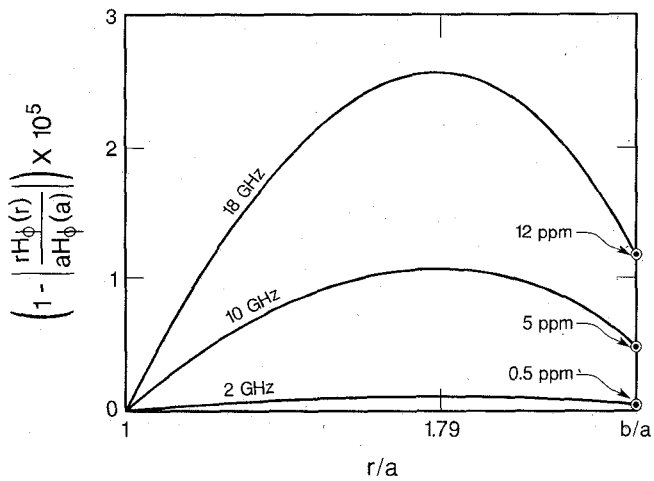

Fig. 9. Graph of the deviation from unity of the magnitude of the normalized magnetic field as a function of frequency.

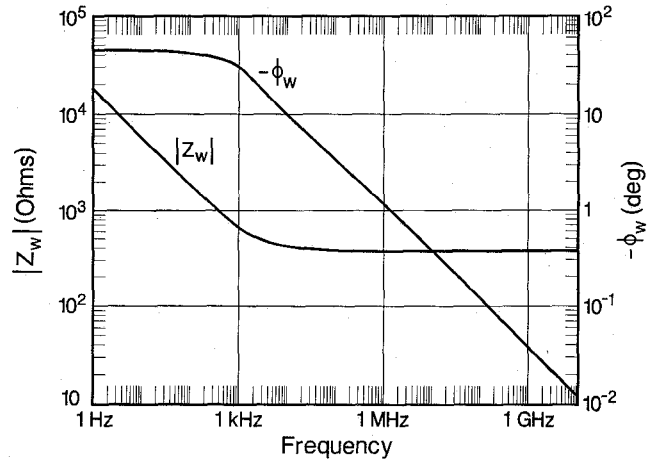

Fig. 10. Graph of the magnitude and phase of the wave impedance between the conductors as a function of frequency.

TABLE III
THE RATIO $|I_1/I_3|$ AT VARIOUS FREQUENCIES

Frequency	$\lvert I_1/I_3\rvert$
18 GHz	1.00001137475840
10 GHz	1.00000471012008
1 GHz	1.00000014894653
100 MHz	1.00000000471004
1 MHz	1.00000000000470
1 kHz	1.00000000000000

Calculated using $h_i = k_i$.

currents are not in general equal; this is true even when the conductors are made of identical materials since the magnitude of the ratio in (53) is still not unity because of conductor losses. In the case of vanishingly small losses ($\rho = 0$ or $\sigma = \infty$), however, both sets of equations, (52) and (53), result in $I_3 = -I_1$.

Fig. 9 illustrates how the magnitude of the field ratio in (53) diverges from unity. This variation is due exclusively to conductor loss since the conductors are assumed to be constructed of the same material for the calculation. The magnitude of the ratio in (53) corresponds to the circled points at the right in the figure for the various frequencies indicated. Examination of these points reveals that the ratio is equal to 1 to within 12 parts per million (ppm) at 18 GHz, 5 ppm at 10 GHz, and 0.5 ppm at 2 GHz, showing that the current ratio rapidly approaches unity as the frequency decreases. Table III also shows this effect.

D. Wave Impedance, Phase Velocity

The wave impedance between the conductors is obtained by reciprocating (14) with $i = 2$:

$$Z_2 = \frac{\omega\mu_2\gamma}{jk_2^2} = \frac{\omega\mu_2\left(1-h^2/k_2^2\right)^{1/2}}{k_2}$$

$$= (\mu_2/\epsilon_2)^{1/2}\left(1-h^2/k_2^2\right)^{1/2} \qquad (54)$$

where (15) has been used to obtain the second expression. Fig. 10 is a graph of the magnitude and phase of this impedance. It is interesting to note that the magnitude is not equal to the free-space impedance (377 Ω) at all frequences, decreasing from a value of approximately 20000 Ω at 1 Hz to the free-space value between 1 kHz and 1 MHz. Equally interesting is the phase of Z_2. The magnitude continues to increase as $f^{-1/2}$ as the frequency decreases while the phase levels out at a negative 45°. The increase in magnitude is due to the fact that the magnitude of the radial electric field remains constant with frequency while the magnetic field magnitude falls off as $f^{1/2}$.

The variation with frequency seen in Fig. 10 vanishes as it should when the line loss disappears, the remaining constant value being the free-space impedance $\sqrt{\mu/\epsilon}$ with zero phase.

Fig. 11 is a graph of the phase velocity

$$v = \frac{\omega}{\mathrm{Im}(\gamma)} \tag{55}$$

of the principal wave as a function of frequency. The $f^{1/2}$ falloff disappears as the line loss vanishes.

VI. Conclusions

An exact solution to Maxwell's equations describing the propagation of the principal mode in a lossy coaxial transmission line has been presented along with a scheme for finding the principal root h of the determinantal equation and the exact propagation constant γ.

Being able to calculate the exact γ provides the first real check on the accuracy of the microwave and full range approximations to the propagation constant. The $\hat{\gamma}$ curves in fig. 8 show that the full range approximation is highly accurate over the entire usable frequency range of the line while the microwave approximation suffers a large relative error at frequencies below about 1 MHz. It should be noted, however, that the γ_0 loss and angle error curves show absolute errors less than 2×10^{-6} dB/cm and 10^{-6} deg/cm respectively at these lower frequencies, values that may be sufficiently small for most practical purposes even though the relative errors are large.

Approximate expressions for the fields between the conductors were presented that satisfy Maxwell's equations to first order in h^2. The errors in these expressions are shown in Table II.

It is often assumed that the principal mode wave impedance for the fields between the conductors is equal to the free-space value $\sqrt{\mu/\epsilon}$. Fig. 10 shows that this assumption is significantly in error below approximately 1 MHz when the line is lossy.

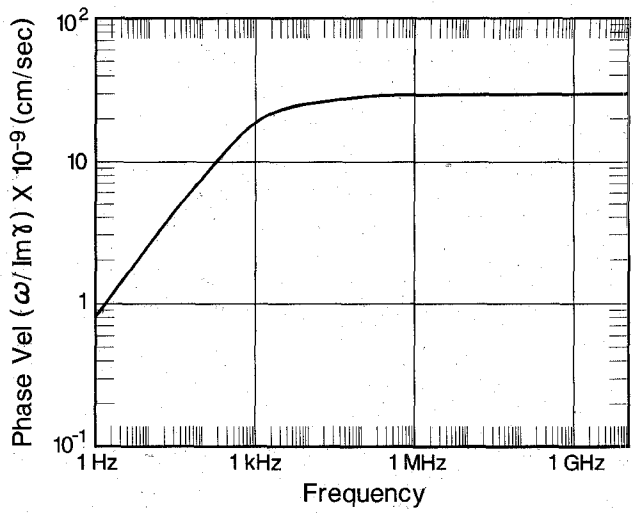

Fig. 11. Graph of the phase velocity as a function of frequency.

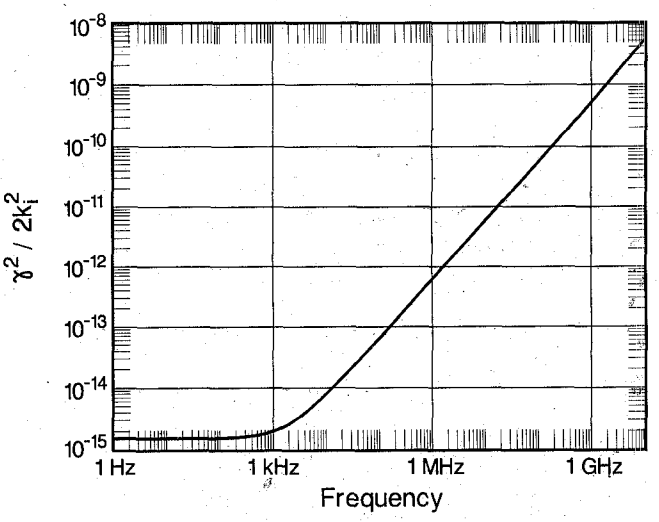

Fig. 12. Graph of $\gamma^2/2k_i^2$ as a function of frequency.

Appendix
Approximations for $R_1(h_1a)$ and $R_3(h_3b)$, Surface Impedance

The approximations ($i = 1$, 3, and $r = a, b$)

$$R_i(h_i r) \doteq R_i(k_i r) \tag{A1}$$

are sufficiently accurate to be used without concern, and make calculations like (37) easier because the right side of (A1) does not depend on the solution h of the determinantal equation (28). The corresponding error from replacing h_i with k_i will be discussed first and then the surface impedance.

From (12),

$$h_i = k_i\left(1+\frac{\gamma^2}{k_i^2}\right)^{1/2} \tag{A2}$$

and calculations show (see Fig. 12) that the second factor on the right is equal to 1 to better than six parts in 10^9. Thus, for practical purposes,

$$h_i = k_i. \tag{A3}$$

From (13),

$$k_i = (\omega\mu_i\sigma_i)^{1/2}\left(1+\omega^2\epsilon_i^2/\sigma_i^2\right)^{1/4} \cdot\exp\left[-j\left(\frac{\pi}{4}-\frac{1}{2}\arctan(\omega\epsilon_i\sigma_i)\right)\right]. \tag{A4}$$

The second factor in this equation is equal to 1 to better than two parts in 10^{17} while the increment to $\pi/4$ is no larger than 6×10^{-6} degrees for all lines. Thus,

$$k_i = (\omega\mu_i\sigma_i)^{1/2}e^{-j\pi/4} = k/z_{si} \tag{A5}$$

is an accurate approximation to k_i where k is the free-space wavenumber $2\pi/\lambda$ and z_{si} is the normalized surface impedance of the conductors (see below).

From (A1) and (A5),

$$R_i(h_i a) = R_i(me^{-j\pi/4}) \tag{A6}$$

where m is the magnitude $a\sqrt{\omega\mu_i\sigma_i}$. The function on the right side can be accurately approximated by polynomial fitting if necessary, making its calculation quick and easy.

The normalized surface impedance used in (A5) is the microwave limit of the full range surface impedance derived now. The surface impedances for the inner and outer conductors are defined by [1]

$$Z_{s1} \equiv \frac{E_z(a)}{H_\phi(a)} \qquad Z_{s3} \equiv -\frac{E_z(b)}{H_\phi(b)}. \tag{A7}$$

Using (16), the fields in (9) and (11), and the approximations in (33), (34), and (35) and reducing the result to lowest order in $1/k_i$ leads to

$$z_{s1} \equiv \frac{Z_{s1}}{\sqrt{\mu/\epsilon}} = -j\left(\frac{\epsilon}{\mu}\right)^{1/2} \frac{\omega\mu_2 h}{k_2^2} \frac{Z_0(ha)}{Z_1(ha)} \doteq -j\frac{k}{k_1}\frac{\mu_1/\mu}{R_1(k_1 a)} \tag{A8}$$

and

$$z_{s3} \equiv \frac{Z_{s3}}{\sqrt{\mu/\epsilon}} = j\left(\frac{\epsilon}{\mu}\right)^{1/2} \frac{\omega\mu_2 h}{k_2^2} \frac{Z_0(hb)}{Z_1(hb)} \doteq j\frac{k}{k_3}\frac{\mu_3/\mu}{R_3(k_3 b)} \tag{A9}$$

where the first expressions after the equivalence signs are exact and the last are approximations which are accurate through third order in $\hat{h}$. In the microwave limit where $R_1 = -j$ and $R_3 = j$, (A8) and (A9) reduce to the usual expressions (taking $\mu_1 = \mu_3 = \mu$)

$$z_{s1} = \frac{k}{k_1} \qquad z_{s3} = \frac{k}{k_3} \tag{A10}$$

or (A5). These are the microwave approximations used in the literature for the "surface impedance" or the "normalized surface impedance."

Acknowledgment

The author takes great pleasure in thanking two of his colleagues at the NIST, Dr. R. B. Marks and Dr. D. F. Williams, for carefully checking both the equations presented in the text and the computer software used in generating the results.

References

[1] J. A. Stratton, *Electromagnetic Theory*. New York: McGraw-Hill, 1941.
[2] R. E. Nelson and M. R. Coryell, "Electrical parameters of precision, coaxial, air–dielectric transmission lines," NBS Mono. 96, June 30, 1966.
[3] A. Russell, "The effective resistance and inductance of a concentric main, and methods of computing the Ber and Bei and allied functions," *Phil. Mag.*, vol. 17, pp. 524–552, 1909.
[4] H. A. Atwater, *Introduction to Microwave Theory*. New York: McGraw-Hill, 1962.
[5] W. C. Daywitt, "First-order symmetric modes for a slightly lossy coaxial transmission line," *IEEE Trans. Microwave Theory Tech.*, vol. 38, pp. 1644–1650, Nov. 1990.
[6] J. D. Jackson, *Classical Electrodynamics*. New York: Wiley, 1962.
[7] F. E. Gardiol, *Lossy Transmission Lines*. Norwood, MA: Artech House, 1987.

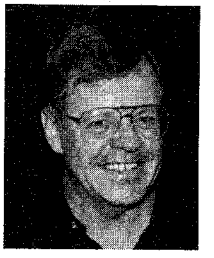

William C. Daywitt was born in Denver, CO, on September 30, 1935. He received the B.S. degree in engineering physics in 1958 and the M.S. degree in applied mathematics in 1959, both from the University of Colorado, Boulder, where he completed most of the graduate work toward the Ph.D. degree in physics.

He joined the staff of the National Bureau of Standards in October 1959. He has worked in the Microwave Calibration Services Section, Engineering Division, Radio Standards Laboratory, Boulder, CO, in the fields of microwave attenuation, microwave noise, and the measurement of earth-terminal G/T. He is presently engaged in developing systems and standards for use in microwave and millimeter-wave noise measurements.